

Orbital-Selective Engineering of Strain-Tunable Chern Insulators in Momentum Space*

Jin Gao, Rongrong Chen,[†] Lei Yang, Zixiong Huang, Dingzhao

Liu, ChengLong Jia,[‡] Li Xi, Desheng Xue, and Kun Tao[§]

Key Laboratory of Magnetism and Magnetic Functional Materials (Lanzhou University), Ministry of Education, Lanzhou, China

(Dated: March 10, 2026)

Unlike conventional approaches where topological order is statically fixed post-synthesis, we demonstrate that a single external knob—strain—can independently modulate topological order and functional responses in the Tc-adsorbed penta-hexa silicene (Tc@PH-Si) monolayer, with both properties governed by a single microscopic mechanism: momentum-space orbital-selective engineering of Tc- d_{xz} /Si- p_x hybridization. Combining first-principles calculations and tight-binding models, we show that biaxial strain drives a complete topological pathway: $C=1$ (0%) \rightarrow $C=0$ (-2%) \rightarrow $C=-1$ (-3% to -4%) \rightarrow $C=0$ metallic state (-6%). This is exemplified by two pivotal states: a topologically critical point yet functionally optimal state at -2% strain ($C=0$) hosting a direct bandgap (0.17 eV) and $d_{11} = 8.34$ pm/V, and a topologically nontrivial but equally optimal state at -4% strain ($C=-1$) with $d_{11} = 11.01$ pm/V—three times that of MoS_2 . Berry curvature analysis reveals that functionality arises from local orbital hybridization strength, while topology originates from its global phase distribution. This establishes a new paradigm for materials design, transforming static functional materials into dynamically tunable quantum platforms.

The discovery of topological quantum states, epitomized by the quantum anomalous Hall insulator (QAHI), has redefined the landscape of condensed matter physics[1–7]. These states host dissipationless chiral edge channels protected by a global topological invariant, the Chern number (C), offering a robust platform for next-generation electronics. Characterized by a non-trivial bulk topological Chern number C , this class of materials is also known as Chern insulators[8]. To date, Chern insulators have been achieved in a variety of two-dimensional systems, such as magnetically doped films $(Bi, Sb)_2Te_3$ [9–13], intrinsic $MnBi_2Te_4$ [14–16], moiré graphene and transition metal dichalcogenide (TMD) heterostructures[17, 18], as well as bilayer V_2O_3 , the V_2MX_4 monolayer, and the M_2X_2 family[19–26]. The capability of dynamically controlling both the sign and magnitude of the Chern number in the topological insulator allows precise control of the propagation direction of chiral edge channels, which is a direct manifestation of the delicate manipulation of the time-reversal symmetry breaking and band structure[27, 28]. This offers great value in driving innovative developments in topological electronics, spintronics, and quantum computing.

However, the field faces a persistent control problem[29]. In most realized materials, the Chern number (C), the fundamental topological invariant, remains static after synthesis, severely limiting applications in reconfigurable quantum devices[30]. Strain engineering is widely seen as a promising way forward, offering a clean and non-invasive way to modify the lattice[31–35]. However, much of the existing work is confined to a relatively elementary level of control: switching between the critical ($C=0$) and topological ($C=\pm 1$) phases[31, 32, 36]. Although recent breakthroughs have successfully realized higher-

Chern-number states in systems such as the bilayer V_2O_3 or the M_2X_2 family[19–25], these states are often “locked in” by specific stacking geometries or elemental compositions[37–42]. Their topological transitions tend to be abrupt, lacking the fine-tuned continuous evolution needed for practical manipulations[43–47].

A more ambitious and technologically relevant goal remains largely unmet: the quantitative stepwise manipulation of the Chern number in a monolayer material using a single continuous external knob such as strain[30]. Or even further, can we use a single knob to independently control what it is (topological order) and what it does (functional response) within a single material? Why is this so difficult? The central challenge lies in the coarse theoretical treatment of strain, which often describes the effect of strain in overly coarse terms as a uniform lattice scaling[37, 48]. This fails to capture how a macroscopic deformation selectively rewrites wavefunctions at specific points in momentum space (k -space) to reshape the global Berry curvature distribution. Recent studies have begun to emphasize the importance of orbital degrees of freedom[38], however, a predictive framework that connects macroscopic strain to the k -resolved orbital response and further to the global topological order remains lacking. While $TbTi_3Bi_4$ exhibits static orbital selectivity [49, 50], and $GdTi_3Bi_4$ displays spin-intertwined charge order [51], actively manipulating these phenomena with an external knob remains a challenge.

To bridge the disconnect between topology and multifunctionality, we demonstrate that a single external knob—biaxial strain—can independently modulate topological order and functional responses in Tc@PH-Si through selective orbital engineering of momentum-space $Tc-d_{xz}/Si-p_x$. The strain drives a complete topological pathway: $C=1$ (0%) \rightarrow $C=0$ (-2%) \rightarrow $C=-1$ (-3%

to -4%) $\rightarrow C = 0$ metallic (-6%). Crucially, the intermediate point $C=0$ at -2% strain hosts a direct band gap (0.17 eV) and a giant piezoelectric response ($d_{11} = 8.34$ pm/V), while the state $C = -1$ at -4% strain achieves $d_{11} = 11.01$ pm / V—three times that of MoS_2 . Berry curvature analysis reveals that functionality arises from the local orbital hybridization strength, whereas topology originates from global phase distribution. This establishes a new paradigm: the transformation of static functional materials into dynamically tunable quantum platforms through a single, unified mechanism.

Monolayer PH-silicene is an intrinsic 2D magnetic semiconductor (P31m space group) with room-temperature stability[52]. Its magnetic order and electronic properties are tunable via strain or stacking without transition-metal doping. Substituting Si with transition metals yields PH-SiX monolayers ($X = Cd, Zn, Bi, Ga, Al$), which exhibits high piezoelectricity (e.g 63.1 pm V^{-1} for PH-SiZn), tunable band gaps (0.11 – 1.07 eV) and a giant Rashba effect in PH-SiBi ($\alpha_R = 1.18$ eV \AA^{-1}), promising for functional devices[53]. Transition-metal adsorption creates PH-SiBiX ($X = Sc$ – Cd), a multifunctional platform[54]. It simultaneously hosts record piezoelectricity ($d_{11} = 13.06$ pm V^{-1} for Ti), auxeticity ($\nu \sim -0.206$ for Ni), strain-tunable visible-light absorption (7.5 – 16%) and strong spin-orbit coupling (~ 50 meV), enabling adaptive piezotronics and flexible optoelectronics.

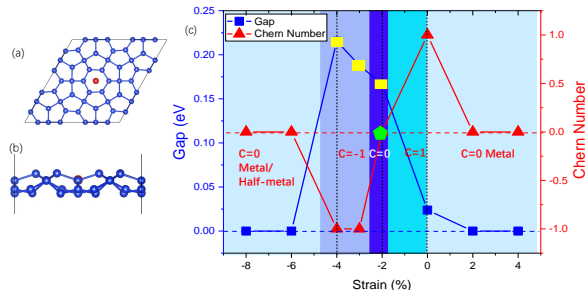


FIG. 1. (a) , (b) Top and side view of the Tc@PH-Si. (c) The evolution of the band gap and the Chern Numbers with the strain. The yellow rectangles marked in the figure denote the direct band gap regions.

Computational details are provided in Sect. A of the *Supplementary Material*. Our strategy for engineering a Chern insulator employs 3d and 4d transition metal atoms adsorbed on PH-silicene (denoted M@PH-Si) motivated by the progress of previous studies in graphene[55].

The lattice stability and magnetic properties of all of the M@PH-Si monolayers are analyzed in Sec. B of the *Supplementary Material*. The evolution of the topological Chern number C with biaxial strain in monolayer Tc@PH-Si is summarized in Fig. 1 (c). At zero strain,

the system is a Chern insulator with $C = +1$. Upon applying compressive strain, we observe a complete topological pathway: $C = +1$ (0%) $\rightarrow C = 0$ (-2%) (topologically critical point) $\rightarrow C = -1$ (-3% to -4%) $\rightarrow C = 0$ (-6%) (metallic state); the $C = 0$ state in the strain -2% is particularly noteworthy, as it marks the closure of the topological gap and the onset of a direct band gap, which remains direct throughout the strain range -2% to -4% [Fig. 1(c), yellow shaded region]. The band gap reaches a maximum of ~ 0.22 eV at -4% strain before closing again at higher compression. This indirect-to-direct shift is critical for optoelectronic performance, as a direct band gap promotes efficient electron-hole recombination, thereby improving light absorption and emission efficiency[56–58].

In particular, this evolution of the band gap is closely correlated with the variation of the Chern number: the system exhibits $|C| = 1$ at 0% , -3% and -4% strain, respectively, while $C = 0$ is observed at -2% strain, indicating that the shift in the character of the band gap (indirect-to-direct) and the modulation of the topological invariants are synergistically regulated by strain. This strong correlation not only reveals the intrinsic link between electronic topological properties and optical performance of the material but also provides a feasible strategy for tuning the topological and optoelectronic properties of the system through strain engineering.

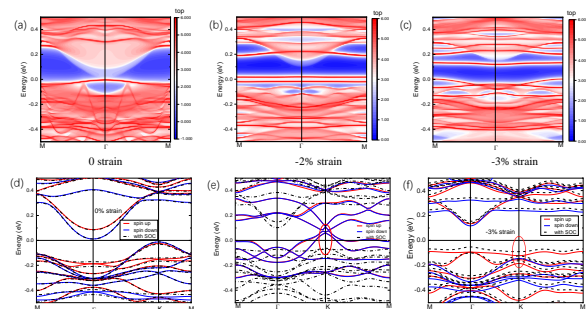


FIG. 2. Surface-projected band structures of the Tc-adsorbed PH-silicene nanoribbon under different strains: (a) 0% strain, (b) -2% and (c) -3%. Electronic structures of Tc@PH-Si under different strains with and without SOC (d) 0% strain, (e) -3% and (f) -4%.

To elucidate the origin of the strain-dependent Chern numbers in Tc@PH-Si, we examined the edge states of the nanoribbons under representative strains of 0% , -2% and -3% , corresponding to Chern numbers $C = 1, 0$ and -1 (Fig. 2). In 0% strain $C = 1$, a single gapless chiral mode appears selectively on one surface of the buckled ribbon [Fig. 2(a)], originating from a band inversion at the Γ point when spin-orbit coupling (SOC) is included [Fig. 2(d)]. A similar single edge state is observed for the $C = -1$ phase under -3% and -4% strain [Fig. 2 (c)]. However, at -2% strain, two edge-like states emerge around

the Fermi level; these are not chiral surface states, as they are strongly localized and are not connected to the conduction or valence bands[Fig. 2 (b)].

However, the bottom surface shows only a diffuse, multi-branch structure near the Fermi level, consistent with boundary asymmetry induced by the puckered lattice; see *the supplementary material*. The intrinsic buckling of PH-silicene, analogous to that in buckled β -Sb monolayers, can promote higher-order topological responses[59] and provides a versatile structural platform for strain-tunable Chern phases in this magnetic system. The selective emergence of a clean one-channel edge spectrum solely on the top surface is robust, and its boundary manifestation is highly sensitive to the local atomic registry—a key design principle for future topological nanodevices.

Figures 2(d)–(f) show the band structures of Tc@PH-Si at 0%, -2% and -3% strain, calculated with and without spin-orbit coupling (SOC). Without SOC, the spin-up bands touch at the Γ point at 0% strain. Including SOC opens substantial gaps at these crossings near the Fermi level. At 0% strain, the GGA-calculated SOC gap is 37.9 meV. Although smaller than the HSE predicted gaps in Bi_2Te_3 [60], $MnBi_2Te_4$ [61] and M_2X_2 [62], it is comparable to the HSE-derived gap in the room-temperature QAHE system TbCl (42.8 meV)[63]. As the compressive strain increases to -4%, a band crossing develops along the Γ -K directions due to threefold rotational symmetry. Consequently, the SOC-induced gap at Γ increases slightly to 45.6 meV, while the gap at K points increases to approximately 60.3 meV.

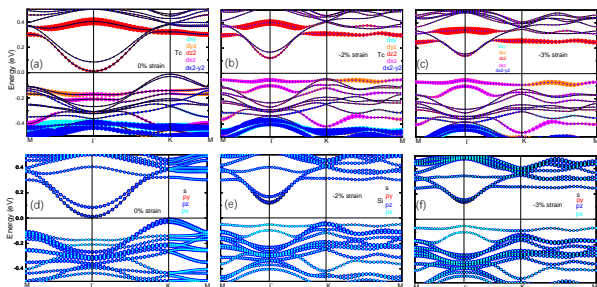


FIG. 3. d -orbital projected band structures of the Tc in the monolayer Tc@PH-Si under different strains: (a) 0%, (c) -3% and (e) -4%; p -orbital projected band structures of the Si in the Tc@PH-Si under different strains: (b) 0%, (d) -3% and (f) -4%. The sizes of the circles indicate the weight of different orbitals.

The quantized Chern number $C = 1$ originates from an orbital selective reconstruction mediated by spin-orbit coupling (SOC). As shown in Fig.2 and Fig.3, SOC does not act as a uniform perturbation but rather as a symmetry-selective manipulator at the Γ point. It lifts the degeneracy of the Si- p_x and Si- p_y states and, more

importantly, induces a pronounced splitting within the active Tc- d_{xz}/d_{yz} manifold. This splitting produces a hybrid orbital that remains degenerate with d_{yz} , while shifting its counterpart to higher energy—an effect that is anisotropic in momentum space due to the inherent d_{xz}/d_{yz} energy separation along the M- Γ path even without SOC. This orbital selective reconstruction directly reorders band energies near the Fermi level, enabling a single band inversion. The resulting momentum-dependent hybridization gives rise to a spatially textured Berry curvature distribution, whose integral over the Brillouin zone is quantized to a Chern number $C = 1$. This establishes a direct link between microscopic orbital reconstruction and the macroscopic topological invariant.

The strains 0% and -3% exhibit surface states with Berry curvature concentrated at K points, the critical strain -2% reveals an orbital-decoupled intermediate state: band structure analysis shows that the Tc d_{xz} and d_{yz} orbitals—hybridized in both $C = \pm 1$ phases—become spatially separated (d_{xz} along Γ -K, d_{yz} along K-M) with negligible mixing of the K point (Fig.2 (b)). This creates fragmented Berry curvature multipoles that geometrically cancel, producing $C \approx 0$ despite local singularities $|\Omega_z| > 10^3 \text{ \AA}^2$, see Fig.5 (d).

We identify this as momentum-space orbital selection, where compressive strain quenches orbital entanglement without gap closing. Unlike conventional band-inversion transitions, the $C \approx 0$ state is topologically critical: Wilson loops show a flat WCC evolution, yet a singular local Berry phase (Fig. 3). The d_{xz} - d_{yz} dephasing enables continuous piezo-topological switching through an off-state, opening avenues for orbital-patterned quantum devices.

To trace the strain-driven evolution of the band structure, we analyze the momentum-resolved orbital-projected bands in the presence of spin-orbit coupling in Fig. 3, which represent a weight decomposition adapted to symmetry rather than exact eigenstates. The physical reliability of evolutionary trends in orbital weights has been cross-validated through COHP bonding analysis (Fig.4). This reveals that the reconfiguration of the Chern number from $C = +1$ to $C = -1$ occurs via a precise two-stage reconfiguration of orbital interactions in momentum space (see the Supplementary Materials). The transition from 0% to -3% strain acts as a topological reset. *At the K point, the dominant character of the highest valence band shifts from Si- p_z (hybridized with p_x/p_y) to strongly coupled Si- p_x/p_y states at the Γ point.* corresponding to a global weakening of key hybridizations: between Si- p_z and Si- p_x/p_y , and between the crucial Tc orbitals d_{xz} and d_{yz} . Simultaneously, the contribution of the Tc d_{z^2} orbital to the conduction-band minimum at Γ decreases. These coordinated changes dismantle the specific orbital network that stabilized the original order $C = +1$. As the strain increases to -2% ($C = 0$), the d_{xz} and d_{yz} orbitals decouple at the K point, leading to a redistribution of the Berry curvature that cancels the net

Chern number. Crucially, the $C=0$ state at -2% strain is not a conventional quantum critical point (where the bandgap closes), but rather a dynamic equilibrium state where Berry curvature contributions from Γ and K points precisely cancel while the bandgap remains open, providing direct evidence that topological phase transitions can proceed through well-defined intermediate states rather than abrupt jumps.

The stabilization of the $C = -1$ phase at -4% strain is orchestrated through a synergistic two-front operation in momentum space. First, at the K point, a new strong coupling emerges between the previously isolated $Tc-d_{xz}$ and d_{yz} orbitals, establishing a fresh channel for band inversion and Berry curvature generation. Second, at the Γ point, the coupling between the $Tc-d_{xy}$ and $d_{x^2-y^2}$ orbitals is dramatically enhanced. *This hybridized manifold shifts upwards by ~ 0.1 eV, amplifying its influence near the Fermi level and reinforcing a pre-existing topological source.* These changes are further corroborated by a pronounced up-shift (~ 0.2 eV) of the $Tc-d_{z^2}$ orbital and a purification of the $Si-p_z$ character at the edge of the conduction-band, collectively enhancing Berry curvature while maintaining $C = -1$.

In essence, biaxial strain functions act as a quantum manipulator in momentum-space. It mirrors the orbital selective physics recently identified in monolayer M_2X_2 systems[62], where the Chern number is determined not by the count of inverted bands at a single k point, but by the symmetry-protected spatial distribution of crossings across the Brillouin zone. The strain-driven orbital engineering in $Tc@PH-Si$ resonates with the orbital selectivity in $TbTi_3Bi_4$ [49], but elevates it from a static property to a dynamic tool. Its multifunctional enhancement mirrors the intertwined orders in $GdT_i_3Bi_4$ [51], yet is orchestrated by a single stimulus.

Crystal orbital Hamiltonian population (COHP) analysis directly links microscopic bonding to macroscopic topology, revealing that the strain-driven topological transition results from a highly selective and spin-dependent reconstruction of specific chemical bonds[64–66].

The strain-dependent integrated COHP (ICOHP) in Fig. 4 quantifies this evolution of the bonding in $Tc@PH-Si$. Under compression (-4% to -8%), the ICOHP for the pair $Tc-d_{xz}/Si-p_x$ (red squares) becomes substantially more negative, signaling a marked strengthening of the covalent bonding—a key driver for stabilization of phase $C = -1$ at -4% . In contrast, the pairs $d_{x^2-y^2}/p_z$ (black squares) and d_{xy}/p_y (blue triangles) show only minor changes, while the s/s interaction (cyan triangles) remains nearly constant. This orbital-specific response confirms that the topology is governed by directional hybridization, $Tc-d$ and $Si-p$ with the channel d_{xz}/p_x playing the dominant role. The non-monotonic strengthening of the compression bonding in d_{xz}/p_x is directly correlated with the transition from a single- k -point ($C = 1$) to

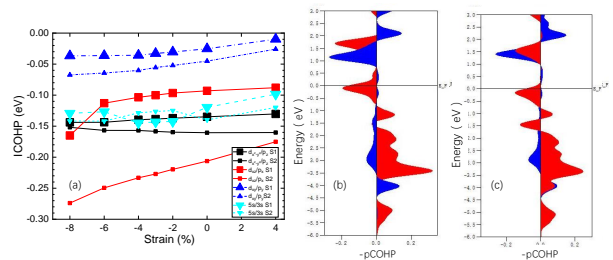


FIG. 4. (a) Strain dependence of ICOHP for various orbital pairs in Tc-adsorbed PH-silicene, in which S_1 (S_2) means spin up (down), respectively. (b) Projected COHP (pCOHP) for $Tc-d_{xz}/Si-p_x$ (red) and $Tc-5s/Si-3s$ (blue) orbital pairs in Tc adsorbed PH-silicene at (left) -4% strain ($C = -1$) and (right) 0% strain ($C = 1$).

a multi- k -point ($C = -1$) inversion of the band, thus establishing a quantitative connection between the bonding and the topological order at the microscopic to macroscopically level.

At -4% biaxial strain, a strain-induced enhancement of orbital hybridization drives $Tc@PH-Si$ into a $C = -1$ Chern insulator. The projected COHP (pCOHP) analysis in Fig. 4(b) identifies the interaction $Tc-d_{xz}/Si-p_x$ as the key driver: under compression, its bonding character (negative pCOHP) intensifies near E_F , while antibonding states shift to higher energies. This strengthened covalent bonding along the x -direction directly modifies band dispersions near high-symmetry points—particularly along $\Gamma-K$ and $\Gamma-M$ —promoting multi- k point band inversions. By contrast, at 0% strain the weaker $Tc-d_{xz}/Si-p_x$ coupling confines the inversion to Γ , resulting in $C=1$.

Specifically, the enhanced bonding of d_{xz}/p_x at -4% strain is precisely correlated with the appearance of two distinct chiral edge modes in the nanoribbon [Fig. 2(c)]—one near E_F and another slightly up—validating the microscopic origin of phase $C = -1$. Unlike previous studies explaining why different materials exhibit static Chern numbers ($C=1$ or 2)[62], this work demonstrates how to engineer a dynamic topological pathway ($C = 1 \rightarrow 0 \rightarrow -1$) within a single material using strain as a continuous external knob. The pathway is governed by a resolved sequential reconfiguration of orbital couplings and establishes a direct quantitative bridge between orbital-specific bonding and macroscopic topological order.

This orbital selective bond response is further confirmed by the spin-antiparallel, non-monotonic evolution of the semi-core $Si-3s/Tc-5s$ interaction (Fig. 4a). Within the 0% to -4% strain range, the ICOHP strengthens for spin-up electrons but weakens for spin-down electrons. This spin-dichotomy signals a profound, global spin-polarized electronic reconstruction. The observa-

tion that even a semi-core s-s interaction far from the Fermi level exhibits such spin-polarized changes underscores that the strain-induced transition $C = 1 \rightarrow C = -1$ involves a global redistribution of spin density across the entire valence manifold, extending well beyond a mere band inversion at the Fermi level. Thus, strain acts as a precision tool for tailoring topology by selectively modulating the strength of key bonds that govern the effective low-energy Hamiltonian. Variations in the lattice constant that modulate the lengths and angles of the Tc-Si bonds, thus quantitatively tuning the specific orbital overlaps of $d-p$.

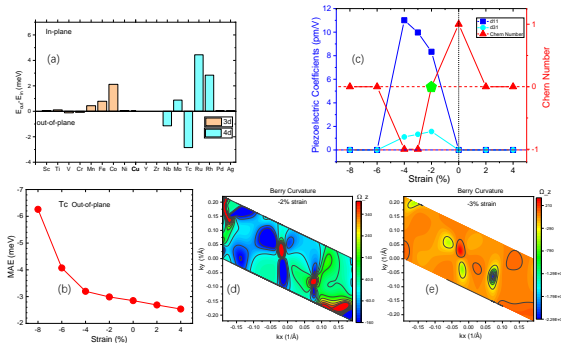


FIG. 5. (a) Magnetic anisotropy energy ($MAE = E_{out} - E_{in}$) for all 3d and 4d transition metals adsorbed on PH-silicene. Negative (positive) values indicate an out-of-plane (in-plane) easy axis; (b) Strain dependence of the magnetic anisotropy energy (MAE) for Tc@PH-Si, with the easy axis along the out-of-plane direction; (c) Strain dependence of the Chern number (red triangles) and piezoelectric coefficients d_{11} (blue squares) and d_{31} (cyan circles) in Tc@PH-Si; (d) and (e) Berry curvature at 0% and -4% strain.

At -4% strain, where the system enters Chern phase $C = -1$, Tc@PH-Si exhibits a large in-plane piezoelectric coefficient $d_{11} \sim 11.5$ pm/V (Fig. 5). This value is approximately three times higher than that of the monolayer $2H-MoS_2$ (3.654 pm/V)[67, 68]—a reference 2D piezoelectric—and significantly exceeds conventional bulk piezoelectrics such as GaN (3.1 pm / V), α -quartz (2.3 pm / V) and AlN (5.1 pm / V)[69–72]. The dramatic enhancement coincides precisely with the topological transition, revealing deep correlations between the orbital-driven band inversion and the lattice-mediated electromechanical response. The compressive strain improves hybridization between the Tc- d_{xz} and Si- p_x orbitals, which simultaneously drives multi-k-point band inversions (along $\Gamma-K$ and $\Gamma-M$) that stabilize the $C = -1$ phase and promotes charge redistribution that amplifies piezoelectric polarization.

In particular, the system also shows a robust out-of-plane piezoelectric response ($d_{31} \sim 1.1$ pm/V at -4% strain), exceeding functionalized h-BN (0.130 pm/V)[73] and $\alpha-In_2Se_3$ (0.415 pm / V)[74]. This coexistence of strong in-plane and out-of-plane piezoelectric-

ity—intrinsically linked to the buckled geometry and magnetic topology—establishes Tc@PH-Si as a unique platform for strain-tunable topo-piezotronic devices, in which quantum transport and mechanical-to-electrical conversion are unified under a single external control. Our work differs from Yu’s established approach[75], where piezoelectricity is used as a probe for topological phase transitions (Z_2) in time-reversal invariant systems, while our work actively engineers piezoelectricity as a tunable functional property in magnetic systems.

We also mapped the magnetic anisotropy energy (MAE) for all 3d and 4d transition metals adsorbed on penta-hexa silicene; see the supplementary material. MAE shows a pronounced dependence on both the d-electron count and the adsorbate period. Among all elements, Tc exhibits the largest MAE out of plane (~ 3.5 meV/Tc-atom), establishing it as the optimal candidate to stabilize perpendicular magnetism on this 2D platform. In general, the 4d series (Y–Ag) displays stronger MAE than the 3d series (Sc–Cu), with Tc showing particularly robust out-of-plane anisotropy.

The MAE of Tc@PH-Si depends strongly and monotonically on the biaxial strain, Fig.5 (b), with the out-of-plane easy axis preserved throughout. Under compression, the MAE becomes increasingly negative, reaching -6.3 meV at -8% strain—a dramatic enhancement of perpendicular magnetic anisotropy that originates from strain-induced modulation of Tc d-orbitals (see *Supplementary material*). Importantly, this MAE enhancement peaks at -4% strain, where the system is in the topological phase $C = -1$, the peak in the piezoelectric response ($d_{11} \sim 11.5$ pm/V) and the indirect-to-direct bandgap transition. This quadruple correlation demonstrates that strain simultaneously and coherently tunes topology, optoelectronic character, magnetism, and electromechanical functionality.

In summary, we have answered the central question posed at the outset: a single external knob—strain—can independently control both the intrinsic topological order and the functional responses within a single material, monolayer Tc@PH-Si. This capability is enabled by momentum-space orbital-selective engineering, where the strain acts as a k-space quantum editor that selectively manipulates the hybridization of $Tc-d_{xz}/Si-p_x$. Berry curvature analysis reveals the underlying mechanism: functionality arises from the local hybridization strength of the orbital, while topology originates from its global phase distribution—a principle that governs the entire evolution driven by strain. Although topologically trivial materials are known for rich functionalities (e.g., GaN for optoelectronics, $BaTiO_3$ for piezoelectricity), the novelty of our work is to elucidate how a single external stimulus dynamically switches topological/critical states while preserving and even enhancing functional properties. The orbital-selective engineering paradigm established here transcends specific mate-

rial systems, providing a general framework for designing dynamically tunable quantum platforms where topology and functionality can be independently optimized through a single external stimulus.

DATA AVAILABILITY

The data supporting the findings of this article are not publicly available after publication because it is not technically feasible and/or the cost of preparing, depositing, and hosting the data would be prohibitive within the terms of this research project. The data are available from the authors upon reasonable request.

* The first three authors contribute equally to this work

† Current address: Henan Institute of Technology, Zhengzhou, China

‡ cljia@lzu.edu.cn

§ taokun@lzu.edu.cn

- [1] F. D. M. Haldane, Model for a quantum hall effect without landau levels: Condensed-matter realization of the "parity anomaly", *Phys. Rev. Lett.* **61**, 2015 (1988).
- [2] R. Yu, W. Zhang, H.-J. Zhang, S.-C. Zhang, X. Dai, and Z. Fang, Quantized anomalous hall effect in magnetic topological insulators, *Science* **329**, 61 (2010).
- [3] H. Weng, R. Yu, X. Hu, X. Dai, and Z. Fang, Quantum anomalous hall effect and related topological electronic states, *Advances in Physics* **64**, 227 (2015).
- [4] K. He, Y. Wang, and Q.-K. Xue, Topological materials: Quantum anomalous hall system, *Annual Review of Condensed Matter Physics* **9**, 329 (2018).
- [5] C.-X. Liu, S.-C. Zhang, and X.-L. Qi, The quantum anomalous hall effect: Theory and experiment, *Annual Review of Condensed Matter Physics* **7**, 301 (2016).
- [6] K. T. A. Tokura, Yoshinori, Yasuda, Magnetic topological insulators, *Nature Reviews Physics* **1**, 126–143 (2019).
- [7] C. Cui-Zu, L. Chao-Xing, and M. A. H., Colloquium: Quantum anomalous hall effect, *Rev. Mod. Phys.* **95**, 011002 (2023).
- [8] D. J. Thouless, M. Kohmoto, M. P. Nightingale, and M. den Nijs, Quantized hall conductance in a two-dimensional periodic potential, *Phys. Rev. Lett.* **49**, 405 (1982).
- [9] C.-Z. Chang, J. Zhang, X. Feng, J. Shen, Z. Zhang, M. Guo, K. Li, Y. Ou, P. Wei, L.-L. Wang, Z.-Q. Ji, Y. Feng, S. Ji, X. Chen, J. Jia, X. Dai, Z. Fang, S.-C. Zhang, K. He, Y. Wang, L. Lu, X.-C. Ma, and Q.-K. Xue, Experimental observation of the quantum anomalous hall effect in a magnetic topological insulator, *Science* **340**, 167 (2013).
- [10] C.-Z. Chang, W. Zhao, D. Y. Kim, H. Zhang, B. A. As-saf, D. Heiman, S.-C. Zhang, C. Liu, M. H. W. Chan, and J. S. Moodera, High-precision realization of robust quantum anomalous hall state in a hard ferromagnetic topological insulator, *Nature Materials* **14**, 473 (2015).
- [11] X. Kou, S.-T. Guo, Y. Fan, L. Pan, M. Lang, Y. Jiang, Q. Shao, T. Nie, K. Murata, J. Tang, Y. Wang, L. He, T.-K. Lee, W.-L. Lee, and K. L. Wang, Scale-invariant quantum anomalous hall effect in magnetic topological insulators beyond the two-dimensional limit, *Phys. Rev. Lett.* **113**, 137201 (2014).
- [12] Y. Ou, C. Liu, G. Jiang, Y. Feng, D. Zhao, W. Wu, X.-X. Wang, W. Li, C. Song, L.-L. Wang, W. Wang, W. Wu, Y. Wang, K. He, X.-C. Ma, and Q.-K. Xue, Enhancing the quantum anomalous hall effect by magnetic codoping in a topological insulator, *Advanced Materials* **30**, 1703062 (2018).
- [13] Y. Deng, Y. Yu, M. Z. Shi, Z. Guo, Z. Xu, J. Wang, X. H. Chen, and Y. Zhang, Quantum anomalous hall effect in intrinsic magnetic topological insulator mnbi2te4, *Science* **367**, 895 (2020).
- [14] C. Liu, Y. Wang, H. Li, Y. Wu, Y. Li, J. Li, K. He, Y. Xu, J. Zhang, and Y. Wang, Robust axion insulator and chern insulator phases in a two-dimensional antiferromagnetic topological insulator, *Nature Materials* **19**, 522 (2020).
- [15] J. Ge, Y. Liu, J. Li, H. Li, T. Luo, Y. Wu, Y. Xu, and J. Wang, High-chern-number and high-temperature quantum hall effect without landau levels, *National Science Review* **7**, 1280 (2020).
- [16] C. Liu, Y. Wang, M. Yang, J. Mao, H. Li, Y. Li, J. Li, H. Zhu, J. Wang, L. Li, Y. Wu, Y. Xu, J. Zhang, and Y. Wang, Magnetic-field-induced robust zero hall plateau state in mnbi2te4 chern insulator, *Nature Communications* **12**, 4647 (2021).
- [17] M. Serlin, C. L. Tschirhart, H. Polshyn, Y. Zhang, J. Zhu, K. Watanabe, T. Taniguchi, L. Balents, and A. F. Young, Intrinsic quantized anomalous hall effect in a moiré heterostructure, *Science* **367**, 900 (2020).
- [18] T. Li, S. Jiang, B. Shen, Y. Zhang, L. Li, Z. Tao, T. Devakul, K. Watanabe, T. Taniguchi, L. Fu, J. Shan, and K. F. Mak, Quantum anomalous hall effect from intertwined moiré bands, *Nature* **600**, 641 (2021).
- [19] S. Mellaerts, R. Meng, M. Menghini, V. Afanasiev, J. W. Seo, M. Houssa, and J.-P. Locquet, Two dimensional v_2o_3 and its experimental feasibility as robust room-temperature magnetic chern insulator, *npj 2D Materials and Applications* **5**, 65 (2021).
- [20] Y. Duan, X. Xu, Y. Mao, X. Niu, H. Lian, X. Yao, J. Lu, A. He, Y. Liu, and X. Zhang, 2d $mntix_2$ ($x=f/cl/br$) monolayers: Robust valley-polarized quantum anomalous hall insulators with high transition temperatures and wide bandgaps, *Applied Physics Letters* **125**, 033101 (2024).
- [21] Y. Li, J. Li, Y. Li, M. Ye, F. Zheng, Z. Zhang, J. Fu, W. Duan, and Y. Xu, High-temperature quantum anomalous hall insulators in lithium-decorated iron-based superconductor materials, *Phys. Rev. Lett.* **125**, 086401 (2020).
- [22] H. Wang and J. Wang, Topological bands in two-dimensional orbital-active bipartite lattices, *Phys. Rev. B* **103**, L081109 (2021).
- [23] L. Liu, H. Huan, Y. Xue, H. Bao, and Z. Yang, Anisotropy-induced phase transitions in an intrinsic half- Chern insulator ni2i2, *Nanoscale* **14**, 13378 (2022).
- [24] Y. Jiang, H. Wang, K. Bao, Z. Liu, and J. Wang, Monolayer v_2MX_4 : A new family of quantum anomalous hall insulators, *Phys. Rev. Lett.* **132**, 106602 (2024).
- [25] S.-D. Guo, Y.-T. Zhu, J.-L. Xin, and B.-G. Liu, Correlation-enhanced spin-orbit coupling in a quantum anomalous hall insulator fe2br2 monolayer with a large band gap and robust ferromagnetism, *J. Mater. Chem. C* **10**, 8381 (2022).

- [26] Y. Jiang, H. Wang, K. Bao, Z. Liu, and J. Wang, Monolayer v_2MX_4 : A new family of quantum anomalous hall insulators, *Phys. Rev. Lett.* **132**, 106602 (2024).
- [27] J. Ding, H. Xiang, J. Hua, W. Zhou, N. Liu, L. Zhang, N. Xin, B. Wu, K. Watanabe, T. Taniguchi, Z. c. v. Sofer, W. Zhu, and S. Xu, Electric-field switchable chirality in rhombohedral graphene chern insulators stabilized by tungsten diselenide, *Phys. Rev. X* **15**, 011052 (2025).
- [28] J. Zheng, S. Wu, K. Liu, B. Lyu, S. Liu, Y. Sha, Z. Li, K. Watanabe, T. Taniguchi, J. Jia, Z. Shi, and G. Chen, Switchable chern insulators and competing quantum phases in rhombohedral graphene moiré superlattices, *Phys. Rev. Lett.* **135**, 136302 (2025).
- [29] Y.-F. Zhao, R. Zhang, R. Mei, L.-J. Zhou, H. Yi, Y.-Q. Zhang, J. Yu, R. Xiao, K. Wang, N. Samarth, M. H. W. Chan, C.-X. Liu, and C.-Z. Chang, Tuning the chern number in quantum anomalous hall insulators, *Nature* **588**, 419 (2020).
- [30] Y.-T. Yao, S.-Y. Xu, and T.-R. Chang, Atomic scale quantum anomalous hall effect in monolayer graphene/mnbi2te4 heterostructure, *Mater. Horiz.* **11**, 3420 (2024).
- [31] S.-D. Guo, W.-Q. Mu, J.-H. Wang, Y.-X. Yang, B. Wang, and Y.-S. Ang, Strain effects on the topological and valley properties of the janus monolayer $vsigen_4$, *Phys. Rev. B* **106**, 064416 (2022).
- [32] E. V. C. Lopes and T. M. Schmidt, Tuning quantum anomalous hall effect in ferromagnetic $1t-crx_2$ ($x=bi, sb$) monolayers, *Applied Physics Letters* **125**, 243103 (2024).
- [33] H. Chen, J. Lu, N. Wang, X. Zhao, G. Hu, X. Yuan, and J. Ren, Strain-induced high-chern-number spin-unlocked edge states in monolayer $mnaso_3$ with intrinsic quantum anomalous hall effect, *Applied Physics Letters* **124**, 153101 (2024).
- [34] Z. Li, Y. Han, and Z. Qiao, Chern number tunable quantum anomalous hall effect in monolayer transitional metal oxides via manipulating magnetization orientation, *Phys. Rev. Lett.* **129**, 036801 (2022).
- [35] Y. Tian, X. Kong, C. Jiang, H.-J. Zhang, and W.-J. Gong, Quantum anomalous layer hall effect in realistic van der waals heterobilayers, *Nano Letters* **25**, 491 (2025).
- [36] L. Zhang, N. Wang, X. Zhao, G. Hu, J. Ren, and X. Yuan, Stacking-tuned quantum anomalous hall effect and multiphase transition in kagome lattice v_2se_3 , *J. Mater. Chem. C* **12**, 16981 (2024).
- [37] W. Sun, X. Li, B. Li, X. Zou, B. Huang, Y. Dai, and C. Niu, Switchable quantum anomalous hall effect in a ferromagnetic topological crystalline insulating npsb monolayer, *Journal of Physics D: Applied Physics* **55**, 305301 (2022).
- [38] R. Bhattarai, P. Minch, Y. Liang, S. Zhang, and T. D. Rhone, Strain-induced topological phase transition in ferromagnetic janus monolayer $mnsbbis_2te_2$, *Phys. Chem. Chem. Phys.* **26**, 10111 (2024).
- [39] H. Bao, B. Zhao, J. Zhang, Y. Xue, T. Zhou, and Z. Yang, Quantum anomalous hall effect with high chern numbers in functionalized square-octagon sb monolayers, *2D Materials* **10**, 035004 (2023).
- [40] W. Zhu, C. Song, H. Bai, L. Liao, and F. Pan, High chern number quantum anomalous hall effect tunable by stacking order in van der waals topological insulators, *Phys. Rev. B* **105**, 155122 (2022).
- [41] A. Du, Y. Tang, L. Kuang, T. Yang, S. Qiu, J. Cai, and C. Yan, Quantum anomalous hall effect with tunable chern number in intrinsic high-temperature ferromagnetic monolayer $mnsbo_3$, *ACS Applied Electronic Materials* **7**, 7301 (2025).
- [42] W. Liang, Z. Li, J. An, Y. Ren, Z. Qiao, and Q. Niu, Chern number tunable quantum anomalous hall effect in compensated antiferromagnets, *Phys. Rev. Lett.* **134**, 116603 (2025).
- [43] J. Wang, B. Lian, H. Zhang, Y. Xu, and S.-C. Zhang, Quantum anomalous hall effect with higher plateaus, *Phys. Rev. Lett.* **111**, 136801 (2013).
- [44] J. Li, X. Cheng, and H. Zhang, Strain-driven topological phase transition in the $oscl_2$ ferrovalley semiconductor, *J. Phys. Chem. C* **129**, 18172 (2025).
- [45] S. Wang, J. Li, L. Wang, L. Meng, A. He, and X. Zhang, Interlayer interaction controllable multiple anomalous hall effect in bilayer janus structures, *Applied Physics Letters* **128**, 032401 (2026).
- [46] S. Ji, C. Quan, R. Yao, J. Yang, and X. Li, Reversal of orbital hall conductivity and emergence of tunable topological quantum states in orbital hall insulators, *Phys. Rev. B* **109**, 155407 (2024).
- [47] Y. Lv, P. Wang, and C. Zhang, Manipulation of intrinsic quantum anomalous hall effect in two-dimensional $moyn_2cscl$ mxene, *Chinese Physics B* **31**, 127303 (2022).
- [48] M. Mannai and S. Haddad, Strain tuned topology in the haldane and the modified haldane models, *Journal of Physics: Condensed Matter* **32**, 225501 (2020).
- [49] E. Cheng, K. Wang, Y. Hao, W. Chen, H. Tan, Z. Li, M. Wang, W. Gao, D. Wu, S. Sun, T. Ying, S. Nie, Y. Li, W. Schnelle, H. Chen, X. Zhou, R. Koban, Y. Chen, B. Yan, Y.-f. Yang, W. Wu, Z. Liu, and C. Felser, Interwoven magnetic kagome metal overcomes geometric frustration, *Nature Materials* 10.1038/s41563-025-02414-4 (2025).
- [50] R. Zhang, B. Yu, H. Tan, Y. Cheng, F. Shen, J. Yang, D. Mu, X. Han, A. Zong, Q. Hu, X. Chen, Y. Hu, C. Meng, J. Ren, J. Li, Z. Chen, Z. Liu, M. Ye, M. Hashimoto, D. Lu, S. Jin, B. Yan, L. He, Z. Wang, T. Shang, Y. Huang, B. Lv, and H. Ding, Observation of orbital-selective dual modulations in an anisotropic antiferromagnetic kagome metal tbt_3bi_4 , *Phys. Rev. X* **15**, 031012 (2025).
- [51] X. Han, H. Chen, Z. Cao, J. Guo, C. Tuo, M.-R. Li, F. Fei, H. Tan, J. Guo, Y. Shi, R. Zhou, R. Wang, Z. Zhao, H. Yang, F. Song, H. Yao, B. Yan, S. Zhu, Z. Wang, and H.-J. Gao, Unconventional spin-intertwined charge density wave in magnetic phases of kagome metal gd_3bi_4 , *Nature Communications* 10.1038/s41467-026-69544-4 (2026).
- [52] K. Tao, R. Chen, J. Kang, D. Xue, V. S. Stepanyuk, and C. Jia, The penta-hexa silicene: A promising candidate for intrinsic room temperature magnetic semiconductor, *Applied Physics Letters* **122**, 212105 (2023).
- [53] L. Yang, J. Gao, R. Chen, C. Jia, D. Xue, and K. Tao, Exploring the electronic and superior piezoelectric properties of two-dimensional ph-six materials for high-performance silicon-based devices, *J. Mater. Chem. C* **12**, 16583 (2024).
- [54] L. Yang, J. Gao, R. Chen, C. Jia, D. Xue, and K. Tao, Strain-responsive ph-sibix monolayers: computational design of multifunctional 2d materials for piezotronic and optoelectronic applications, *J. Mater. Chem. C* **13**, 14787

- (2025).
- [55] J. Ding, Z. Qiao, W. Feng, Y. Yao, and Q. Niu, Engineering quantum anomalous/valley hall states in graphene via metal-atom adsorption: An ab-initio study, *Physical Review B* **84**, 195444 (2011).
- [56] H. Chorsi, B. Cheng, B. Zhao, J. Toudert, V. Asadchy, O. F. Shoron, S. Fan, and R. Matsunaga, Topological materials for functional optoelectronic devices, *Advanced Functional Materials* **32**, 2110655 (2022).
- [57] T. Liu, X. Hong, Z. Lin, J. Qiu, S. Cheng, Y. Lai, Y. Chen, K. He, and J. Yu, Strain engineering of photoinduced anomalous hall effect in topological insulator sb_2te_3 , *Applied Physics Letters* **127**, 053102 (2025).
- [58] D. Leykam, H. Xue, B. Zhang, and Y. D. Chong, Limitations and possibilities of topological photonics, *Nature Reviews Physics* **8**, 55 (2026).
- [59] H. Huang and F. Liu, Higher-order topology induced by structural buckling, *National Science Review* **9**, nwab170 (2021).
- [60] H. Zhang, C.-X. Liu, X.-L. Qi, X. Dai, Z. Fang, and S.-C. Zhang, Topological insulators in bi_2se_3 , bi_2te_3 and sb_2te_3 with a single dirac cone on the surface, *Nature Physics* **5**, 438 (2009).
- [61] D. Zhang, M. Shi, T. Zhu, D. Xing, H. Zhang, and J. Wang, Topological axion states in the magnetic insulator $mnbiz_2te_4$ with the quantized magnetoelectric effect, *Phys. Rev. Lett.* **122**, 206401 (2019).
- [62] Z. Dai, X. Zhu, and L. He, Intrinsic high chern numbers in two-dimensional m_2x_2 materials, *Phys. Rev. Lett.* **135**, 256401 (2025).
- [63] J. Zhong, J. Zhao, J. Zou, and G. Xu, 5d orbital induced room temperature quantum anomalous hall effect in $tbcl$, *npj Computational Materials* **11**, 236 (2025).
- [64] R. Dronskowski and P. E. Bloechl, Crystal orbital hamilton populations (cohpp): energy-resolved visualization of chemical bonding in solids based on density-functional calculations, *The Journal of Physical Chemistry* **97**, 8617 (1993).
- [65] V. L. Deringer, A. L. Tchougréeff, and R. Dronskowski, Crystal orbital hamilton population (cohpp) analysis as projected from plane-wave basis sets, *The Journal of Physical Chemistry A* **115**, 5461 (2011), pMID: 21548594.
- [66] R. Nelson, C. Ertural, J. George, V. L. Deringer, G. Hautier, and R. Dronskowski, Lobster: Local orbital projections, atomic charges, and chemical-bonding analysis from projector-augmented-wave-based density-functional theory, *Journal of Computational Chemistry* **41**, 1931 (2020).
- [67] K.-A. N. Duerloo, M. T. Ong, and E. J. Reed, Intrinsic piezoelectricity in two-dimensional materials, *The Journal of Physical Chemistry Letters* **3**, 2871 (2012).
- [68] W. Wu, L. Wang, Y. Li, F. Zhang, L. Lin, S. Niu, D. Chenet, X. Zhang, Y. Hao, T. F. Heinz, J. Hone, and Z. L. Wang, Piezoelectricity of single-atomic-layer mos_2 for energy conversion and piezotronics, *Nature* **514**, 470 (2014).
- [69] R. Bechmann, Elastic and piezoelectric constants of alpha-quartz, *Phys. Rev.* **110**, 1060 (1958).
- [70] K. Tsubouchi and N. Mikoshiba, Zero-temperature-coefficient saw devices on aln epitaxial films, *IEEE Transactions on Sonics and Ultrasonics* **32**, 634 (1985).
- [71] C. M. Lueng, H. L. W. Chan, C. Surya, and C. L. Choy, Piezoelectric coefficient of aluminum nitride and gallium nitride, *Journal of Applied Physics* **88**, 5360 (2000).
- [72] A. Hangleiter, F. Hitzel, S. Lahmann, and U. Rossow, Composition dependence of polarization fields in $gainn/gan$ quantum wells, *Applied Physics Letters* **83**, 1169 (2003).
- [73] M. Noor-A-Alam, H. J. Kim, and Y.-H. Shin, Dipolar polarization and piezoelectricity of a hexagonal boron nitride sheet decorated with hydrogen and fluorine, *Phys. Chem. Chem. Phys.* **16**, 6575 (2014).
- [74] L. Hu and X. Huang, Peculiar electronic, strong in-plane and out-of-plane second harmonic generation and piezoelectric properties of atom-thick α - m_2x_3 ($m = ga, in; x = s, se$) role of spontaneous electric dipole orientations, *RSC Adv.* **7**, 55034 (2017).
- [75] J. Yu and C.-X. Liu, Piezoelectricity and topological quantum phase transitions in two-dimensional spin-orbit coupled crystals with time-reversal symmetry, *Nature Communications* **11**, 2290 (2020).